ACS SyntheticBiology

pubs.acs.org/synthbio

Research Article

Characterization of Eight Bacterial Biosensors for Microbial Diagnostic and Therapeutic Applications

Troels Holger Vaaben, Ruben Vazquez-Uribe,* and Morten Otto Alexander Sommer*

Cite This: *ACS Synth. Biol.* 2022, 11, 4184–4192

Read Online

ACCESS | Metrics & More | Article Recommendations | Supporting Information

ABSTRACT: The engineering of microbial cells to produce and secrete therapeutics directly in the human body, known as advanced microbial therapeutics, is an exciting alternative to current drug delivery routes. These living therapeutics can be engineered to sense disease biomarkers and, in response, deliver a therapeutic activity. This strategy allows for precise and self-regulating delivery of a therapeutic that adapts to the disease state of the individual patient. Numerous sensing systems have been characterized for use in prokaryotes, but a very limited number of advanced microbial therapeutics have incorporated such sensors. We characterized eight different sensors that respond to physiologically relevant conditions and molecules found in the human body in the probiotic strain *Escherichia coli* Nissle 1917. The resulting sensors were characterized under aerobic and anaerobic conditions and were demonstrated to be functional under gut-like conditions using the nematode *Caenorhabditis elegans* as an in vivo model. We show for the first time how a biosensor is able to detect in vivo the bile acid-like molecule Δ^4-dafachronic acid, a small molecule in *C. elegans* that regulates lifespan. Furthermore, we exemplify how bacterial sensors can be used to dynamically report on changes in the intestinal environment of *C. elegans*, by demonstrating the use of a biosensor able to detect changes in lactate concentrations in the gut lumen of individual *C. elegans*. The biosensors presented in this study allow for dynamic control of expression in vivo and represent a valuable tool in further developing advanced microbiome therapeutics.

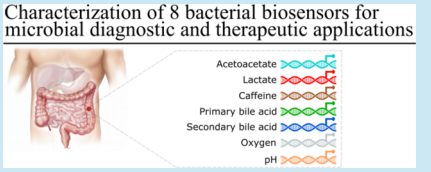

KEYWORDS: *biosensors, microbiome, C. elegans, E. coli Nissle 1917, genetic circuits, bile acids*

INTRODUCTION

The human microbiota is increasingly considered as a pseudo-organ, which is implicated in many aspects of both human health and disease.[1] Accordingly, manipulating the microbiome for therapeutic purposes is of increasing interest.[2] Several avenues are explored for additive or subtractive strategies to manipulate the microbiota with a specific medical goal. These approaches range from the use of specialized dietary approaches to stimulate the growth of beneficial bacteria, known as prebiotics,[3] to the transfer of whole microbial communities from fecal matter of healthy donors into patients with a dysbiotic microbiota, as seen in patients with recurrent *Clostridium difficile* infections.[4] More recently, scientists have begun exploring the rational design of genetically engineered commensal bacteria modified to produce therapeutic molecules of interest,[5] which we refer to as advanced microbiome therapeutics (AMTs). Such cell-based therapeutics have been explored for several indications, including treatment and diagnosis of inflammation[6] metabolic diseases[7] and even cancer.[8]

The use of synthetic biology allows the construction of genetic circuits that can detect and respond to an input of interest. In particular, AMTs could be programmed with such genetic circuits to sense disease biomarkers and deliver therapeutics with site and dose specificity. This on-demand drug release is an attractive attribute of AMTs that could potentially enable an entirely novel therapeutic paradigm, in which drugs are delivered by self-regulating microbial cells that adapt to the precise disease state of an individual patient.[9,10] Bacterial biosensors have also been explored as diagnostic tools to detect the presence of pathological biomarkers in clinical samples[11,12] as a cost-effective solution to point-of-care diagnosis. Recent work has also demonstrated the feasibility of implementing bacterial biosensors in ingestible chips to wirelessly report on biomarkers in the intestine.[13] This technology could be used to closely monitor metabolites and conditions in the intestine in real time and used for diagnostic and research purposes.

In recent years, the genetic toolbox of promoters[14] and sensing elements[15,16] has been greatly expanded. Yet, identifying and integrating the appropriate sensor for a given application remains a challenging task. Often the performance of sensing circuits is solely evaluated under aerobic conditions, which is of limited relevance to applications in the anaerobic environment found throughout most of the human gastrointestinal (GI) tract. Furthermore, many biosensors are operated on high copy number plasmids associated with an

Received: September 9, 2022
Published: November 30, 2022

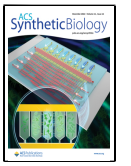

https://doi.org/10.1021/acssynbio.2c00491
ACS Synth. Biol. 2022, 11, 4184–4192

increased metabolic burden on the host and genetic instability,[17] hampering their use for in vivo production of biomolecules. In this work, we provide a set of well-characterized vectors for biosensing relevant molecules and conditions in vivo. The biosensors are integrated on a pMUT1-based plasmid determined to pose minimal metabolic burden and allow high stability in vivo.[18] The plasmids have been deposited in Addgene together with detailed plasmid maps and sequences (Figure S7), expanding the toolbox for research in EcN for in vivo applications.

RESULTS

Construction and Functional Characterization of pMUT-Based Biosensor Plasmids. The necessary genetic elements for the eight biosensors were cloned individually in a single pMUT-1-based plasmid native to EcN (Table 1 and Figure S1). The coding sequences of the necessary transcription factors were placed adjacent to the promoter and reporter gene in the opposite transcription direction to ensure insulation of the reporter gene and its promoter (Figure 1a). The red fluorescent protein mCherry was used as a reporter gene to quantify gene expression levels. The strain of EcN used for this work harbors a constitutively expressed superfolder GFP (sfGFP) integrated in the genome, allowing for a ratiometric normalization of the mCherry reporter signal, in cases where optical density cannot be used as a reliable measure of growth (i.e., when the growth medium is opaque from high concentrations of inducers). The dynamics of each sensor were investigated by exposing cells of EcN harboring the various plasmids to different concentrations of inducers under aerobic and anaerobic conditions. The OD_{600}, mCherry, and sfGFP signal were recorded for 40 h of growth. The mCherry signal was normalized to the OD_{600} to account for differences in growth parameters when exposed to the various compounds, and the gene expression in the normalized relative fluorescence unit (RFU) was used to parameterize the performance of each sensor (Table 2).

Table 1. Biosensors Selected for Use In Vivo

sensor input	regulation	plasmid name	ref.	Addgene ID
acetoacetate	activator	*pAto*	19	192858
lactate	activator	*pLac*	20	192859
caffeine	activator	*pCaf*	21	192860
taurocholic acid	activator	*pTcpP*	11	192861
deoxycholic acid	activator	*pVtrA*	11	192862
lithocholic acid	activator	*pVtrA*	11	192862
oxygen	repressor	*pFF-41.5*	22	192863
oxygen	repressor	*pF8*	23	192864
pH	activator	*pCadBA*	24	192865

All sensors showed a dose-dependent response when exposed to their cognate inducer (Figure 1b). The lactate sensor *pLac* had a dynamic range of 5.7 under aerobic conditions and 2.2 under anaerobic conditions, indicative of oxygen-related gene regulation of this circuit, which has also been reported elsewhere.[25] The highest dynamic range was observed for the secondary bile acid sensor *pVtrA* when exposed to lithocholic acid, with a 32-fold increase. Cells of *EcN* failed to grow in anaerobic conditions when exposed to concentrations of deoxycholic acid higher than 10^{-1} mM, and no activation of the sensor was observed at this concentration.

Sensors for acetoacetate, lactate, caffeine, and secondary bile acid had an operational range that falls within the concentrations found in the human body. The primary bile acid sensor was only activated at concentrations >2 mM taurocholic acid, which exceeds the normal range of concentrations found in the human body. The *pCaf* sensor was also tested against another methylxanthine. As these molecules only differ from caffeine in a single methyl residue, we hypothesized that this sensor could also be activated by other methylxanthines. We saw a robust induction of this sensor in the presence of 0.1 mM theophylline (Figure S2), demonstrating that this sensor could also be employed to sense the downstream metabolites of caffeine.

Both oxygen biosensors follow a similar pattern of expression, with a clear increase in expression levels under anaerobic conditions (Figure 1c). The expression levels remained stable over the 24-h period in aerobic conditions, but the baseline expression (or leakiness) was around 2.5 times higher for *EcN-pF8*. After 24 h, the difference between aerobic and anaerobic expression levels was similar for both biosensors, with *EcN-pF8* and *EcN-pFF-41.5* showing a fold-increase of ∼4 and 3.6, respectively (Figure 1c).

At pH 5, we observed a ∼2-fold increase in expression levels from the pH sensitive pCadC promoter when compared to expression levels at pH 7, both under aerobic and anaerobic conditions (Figure 2d). The output from this promoter was, however, relatively low compared to the other biosensors at max induction and could be further optimized by changing the promoter or ribosome-binding site. We also controlled for any activation from the acetic acid used to buffer the media to pH 5 and saw no activation of the sensor when grown in pH 7 spiked with acetic acid (Figure S3).

EcN Biosensors Are Stable and Functional In Vivo. As the motivation for this work was to expand the repertoire of biosensors available for use in vivo, it was imperative to prove their functionality under gut-like conditions. To this end, we employed the model organism *Caenorhabditis elegans* due to its ease of use and recent development as a model for characterizing whole-cell bacterial biosensors in vivo.[31] The wild-type strain of *C. elegans* was able to grow and replicate on all EcN biosensor strains tested, with no physiological alterations observed. *C. elegans* was maintained monoxenically on EcN biosensor strains for 5 days to allow colonization. Subsequently, animals were washed and split to nematode growth medium (NGM) plates containing the relevant inducer (+) or a negative control without any inducer (−). To increase the throughput capacity of this system, we sought to employ a live-cell analysis system to image animals, as this would allow the imaging of several animals simultaneously. The use of this imaging system proved successful in its capacity to image multiple animals. A clear difference in the mCherry signal was observed in exposure to the relevant inducer for all biosensors tested, demonstrating the functionality of the biosensors under gut-like conditions. This highlights the fact that cells of EcN located within the intestine of *C. elegans* can detect and respond to the changes in the intestinal environment (Figure 2).

The two oxygen biosensors *pF8* and *EcN-pFF-41.5* were imaged using fluorescence microscopy (Figure 2g,h) to obtain a higher resolution, allowing us to better study the different GI comportments of *C. elegans*. Under aerobic conditions, both biosensors were completely inactive throughout the GI tract, indicating the presence of oxygen through the entire length of

https://doi.org/10.1021/acssynbio.2c00491
ACS Synth. Biol. 2022, 11, 4184−4192

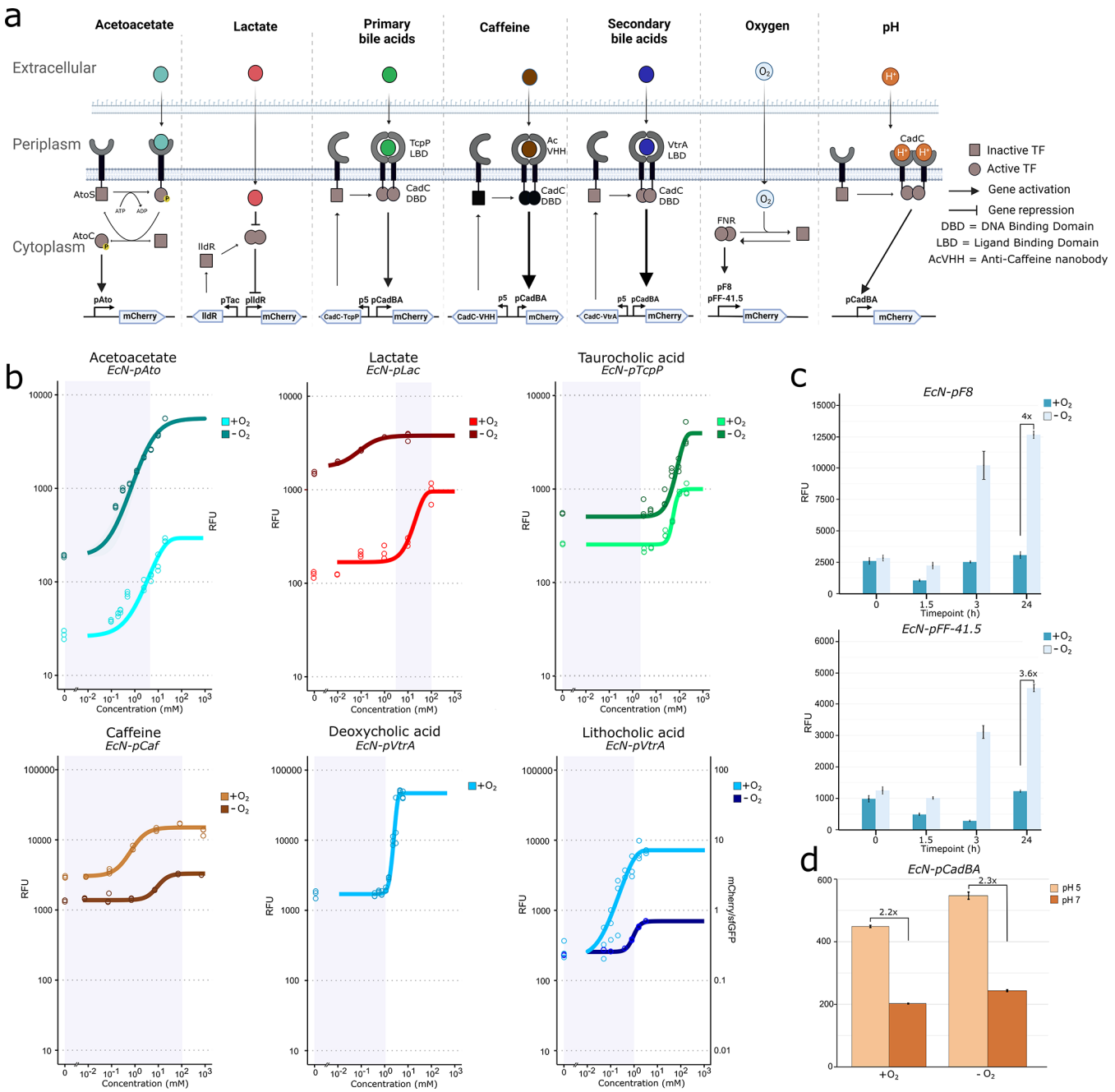

Figure 1. Design and performance of in vivo biosensors in *E. coli* Nissle 1917. (a) Regulatory mechanism and design of in vivo biosensors. (b) Response profiles of in vivo biosensors responding to signal molecules under aerobic ($+O_2$) or anaerobic ($-O_2$) conditions. Lines represent the best fit to a four-parameter log-logistic model, calculated from the mean of three biological replicates in the presence of different concentrations of inducer (circles) computed from normalized mCherry signal after 40 h of growth. Response activation of *EcN-pVtrA* with lithocholic acid was normalized against sfGFP due to opacity of the medium. Shaded area behind graphs indicates the physiologically relevant concentrations of small molecules for acetoacetate[26] (serum), lactate[27] (stool), taurodeoxycholic acid (duodenal content),[28] caffeine[29] (serum), deoxycholic acid[28,30] (duodenal content), and lithocholic acid[28,30] (duodenal content). Quantified response parameters are summarized in Table 2. (c) Response of the two oxygen-regulated promoters *pF8* and *pFF-41.5* at 0, 1.5, 3, and 24 h after transfer from an aerobic culture to either aerobic or anaerobic conditions. (d) Response of the pH-sensitive promoter *pCadBA* after 4 h of growth in lysogeny broth (LB) buffered to pH 5 and pH 7 in aerobic and anaerobic conditions.

the GI tract. This is an important finding, as the levels of oxygen in the intestinal environment of *C. elegans* are still being debated.[32] When exposed to anaerobic conditions for 24 h, we observed a homogeneous induction of the oxygen biosensors throughout the length of the GI tract.

C. elegans was also colonized with pH-sensitive *EcN-pCadBA*, but we saw no signal in any of the animals imaged (Figure S5). The in vitro characterization showed that the activation of this sensor was low compared to the other biosensors, and therefore, the lack of fluorescence is likely to be a result of the low activation state of the biosensor.

EcN strains encoding the biosensors were activated in *C. elegans* when the corresponding molecule was added to the plate (Figure 2). Interestingly, worms colonized with *EcN-VtrA*

https://doi.org/10.1021/acssynbio.2c00491
ACS Synth. Biol. 2022, 11, 4184−4192

Table 2. Dose−Response Parameters of EcN Biosensors

ligand	sensor	y_{max} (RFU)		y_{min} (RFU)		dynamic range		EC_{50} (mM)		cooperativity (k)	
		$+O_2$	$-O_2$	$+O_2$	$-O_2$	$+O_2$	$-O_2$	$+O_2$	$-O_2$	$+O_2$	$-O_2$
acetoacetate	*pAto*	274	5500	26	188	10.5	29.3	11.8	4.13	0.92	1
lactate	*pLac*	933	3772	165	1750	5.7	2.2	33	0.12	1.5	1.1
taurocholic acid	*pTcpP*	976	3900	250	796	3.9	5	58	115	1.2	4.2
caffeine	*pCaf*	13,784	2595	2410	1384	5.3	2.4	1.5	0.011	1	1.8
deoxycholic acid	*pVtrA*	46,955		1735		27		2.9		4.9	
lithocholic acid	*pVtrA*	7048	0.7[a]	215	0.26[a]	32	2.7	0.7	4.35	1.2	3

[a]Normalized to sfGFP signal due to turbidity of the medium.

without addition of any secondary bile acids also showed a strong fluorescence (Figure 2e,f), especially in the intestinal area immediately adjacent to the pharynx. To investigate whether the sensor was responding to an endogenous bile acid-like molecule in *C. elegans*, or whether it was simply an experimental artifact arising from leakiness of the biosensor, an in vitro assay with the *C. elegans* bile acid-like molecule was carried out. Cells of *EcN-VtrA* were exposed to Δ^4-dafachronic acid derived from *C. elegans*, and the response function was monitored. Indeed, the secondary bile acid sensor *EcN-pVtrA* demonstrated a clear dose-dependent increase in mCherry output (Figure S4). This indicates that the *EcN-VtrA* biosensor was able to detect and report on endogenous levels of bile acid-like molecules in *C. elegans*, as observed for worms grown on *EcN-pVtrA* without the addition of any external secondary bile acids.

Detecting Dynamic Changes in the Intestinal Environment of *C. elegans*. The ability to sense and respond to an endogenous molecule of *C. elegans* prompted us to further investigate the ability of utilizing our biosensors to study the metabolism and physiology of bacterivorous nematodes in real time. Arsenite has previously been reported to uncouple mitochondrial respiration and induce a Warburg-like effect in *C. elegans*.[33] High concentrations of arsenite disrupt the mitochondrial membrane potential and stabilize hypoxia-inducible factor 1-alpha (HIF-α) in its active state, leading to an upregulation of the genes involved in glycolysis.[33] This ultimately leads to buildup of intracellular lactate as a consequence of the increased glycolytic flux (Figure 3a). We hypothesized that our bacterial lactate biosensor could be used to report on such changes in situ and individually, instead of mass cultivation of *C. elegans* coupled with mass spectrometry, as is usually employed to study *C. elegans* metabolism.[33,34] Animals were monoxenically grown with the *EcN-pLac* biosensor strain and allowed to grow for 5 days. Animals were then transferred to a fresh NGM plate or NGM plate containing 0.5 mM arsenite for 24 h and imaged using fluorescence microscopy. Exposure to arsenite led to a clear increase in mCherry expression in all animals observed along the whole length of the intestine, with little baseline expression in animals not exposed to arsenite (Figure 3c). The MFI was ∼3 times higher in worms exposed to 0.5 mM arsenite (Figure 3b), clearly indicating an increase in intestinal lactate concentrations and concomitant activation of the lactate biosensor. We also tested if arsenite itself was able to induce *pLac* but saw no activation of the sensor in the presence of 0.5 mM arsenite in vitro (Figure S6). We find this to be a good demonstration of how whole-cell biosensors can be used to study the physiology of individual *C. elegans* in real time, a concept which could be expanded upon by developing biosensors specifically for *C. elegans* research.

DISCUSSION

The sensors for acetoacetate, lactate, caffeine, primary, and secondary bile acids all showed a dose-dependent increase in activity, both under aerobic and anaerobic conditions (Figure 1b). In response to anaerobic conditions, the metabolism of EcN undergoes a plethora of transcriptional regulations from direct gene modulation by oxygen-sensitive transcription factors[35] to more mechanistically indirect regulation such as competition for the RNA II polymerase from alternative sigma factors.[36] The differences in the performance when characterized in aerobic and anaerobic conditions (Table 2) clearly demonstrate the importance of characterizing biosensors in the relevant conditions in which they are to be employed and that oxygen availability is one crucial aspect that can affect the behavior of genetic parts in whole-cell biosensors.

All sensors except the primary bile acid sensor *EcN-pTcpP* were responsive in a range of concentrations within physiologically relevant levels, meaning that they could be tested for use in vivo in humans without further modifications, to sense and respond to relevant biomolecules. In general, a crucial impediment to the application of any biosensors is the fact that information on physiologically relevant concentrations in the intestine is scarce due to the inaccessible nature of sampling in this area and the fact that concentrations vary greatly within individuals. This could be problematic when coupling the production of a therapeutic to pathophysiological biomarkers. As previously mentioned, a recent paper by Inda et al.[13] demonstrated how bacterial sensors can be incorporated into small ingestible devices that wirelessly transmit a signal in response to the presence of specific biomarkers. The biosensors developed in this study could be incorporated into such a system. This technology could dramatically increase our understanding of the chemical composition in the GI tract, by allowing noninvasive and real-time monitoring of biomarkers in both healthy and diseased individuals.

In this study, we employed the model organism *C. elegans* to validate the functionality of the biosensors under gut-like conditions. In the intestinal environment of *C. elegans*, the bacterial cells are exposed to a plethora of stressful physical and chemical conditions,[37] which in turn affects the behavior of the bacterial cells. The transcriptomic profile of *E. coli* K12 when grown in vitro and in vivo in *C. elegans* only shows 47% similarity,[38] highlighting how this small and easily implemented model organism can be used to characterize biosensors in a context that is greatly different from those found when grown in vitro. By colonizing *C. elegans* with biosensing EcN and exposing them to the concentrations that gave rise to the highest level of induction in vitro, we were able to induce a clear response for all small-molecule sensors. Thus, we were

https://doi.org/10.1021/acssynbio.2c00491
ACS Synth. Biol. 2022, 11, 4184−4192

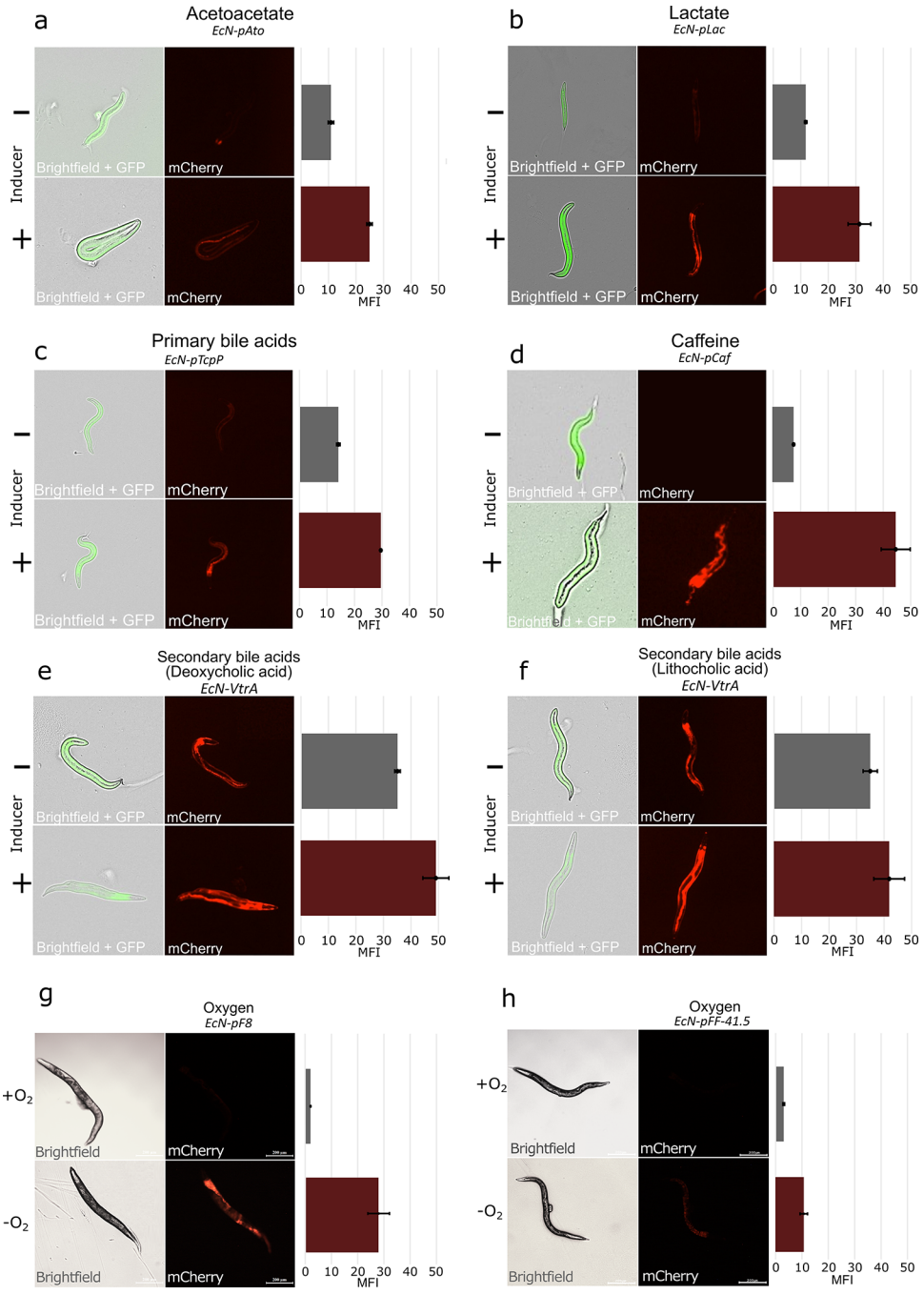

Figure 2. In vivo biosensing in *C. elegans*. Representative images of *C. elegans* N2 colonized with strains of EcN biosensors in the presence (+) or absence (−) of inducer molecules. Bars represent mean fluorescence intensity (MFI) in the red channel, calculated from triplicates. Five adult worms were transferred from NGM plates containing engineered EcN strains onto NGM plates containing (a) 20 mM acetoacetate, (b) 100 mM lactate, (c) 186 mM taurocholic acid, (d) 77 μM caffeine, (e) 5.2 mM deoxycholic acid, and (f) 3.2 mM lithocholic acid. After 24 h on induction plates, three adult worms were transferred to a separate NGM plate containing 1 mM levamisole as the anesthetic and imaged using a IncuCyte S3 Live-Cell Analysis System with a 4× objective and 300 ms exposure for red and green fluorescence images. (g,h) Worms were colonized with EcN biosensors responsive to oxygen and split into aerobic and anaerobic conditions. After 24 h, three adult worms from each condition were imaged using fluorescence microscopy.

able to prove the functionality of all circuits under gut-like conditions.

Interestingly, in characterizing the biosensor for human secondary bile acids (*EcN-VtrA*), we discovered that it was able to sense and respond to the presence of an endogenous bile acid-like molecule, Δ^4-dafachronic. This molecule is involved in controlling lifespan, lipid metabolism, and dauer formation in *C. elegans* and other nematodes.[39,40] Current methods for quantification of sterols in *C. elegans* rely on highly specialized and labor-intensive procedures such as gas chromatography-tandem mass spectrometry, which also require the cultivation of large numbers ($\sim 10^5$) of animals.[41] The utilization of the *EcN-VtrA* biosensor could allow real-time detection and reporting of dafachronic acid levels in situ and could be used to further elucidate on the role of these bile-acid-like molecules in nematode biology. We further exemplified the use of

https://doi.org/10.1021/acssynbio.2c00491
ACS Synth. Biol. 2022, 11, 4184−4192

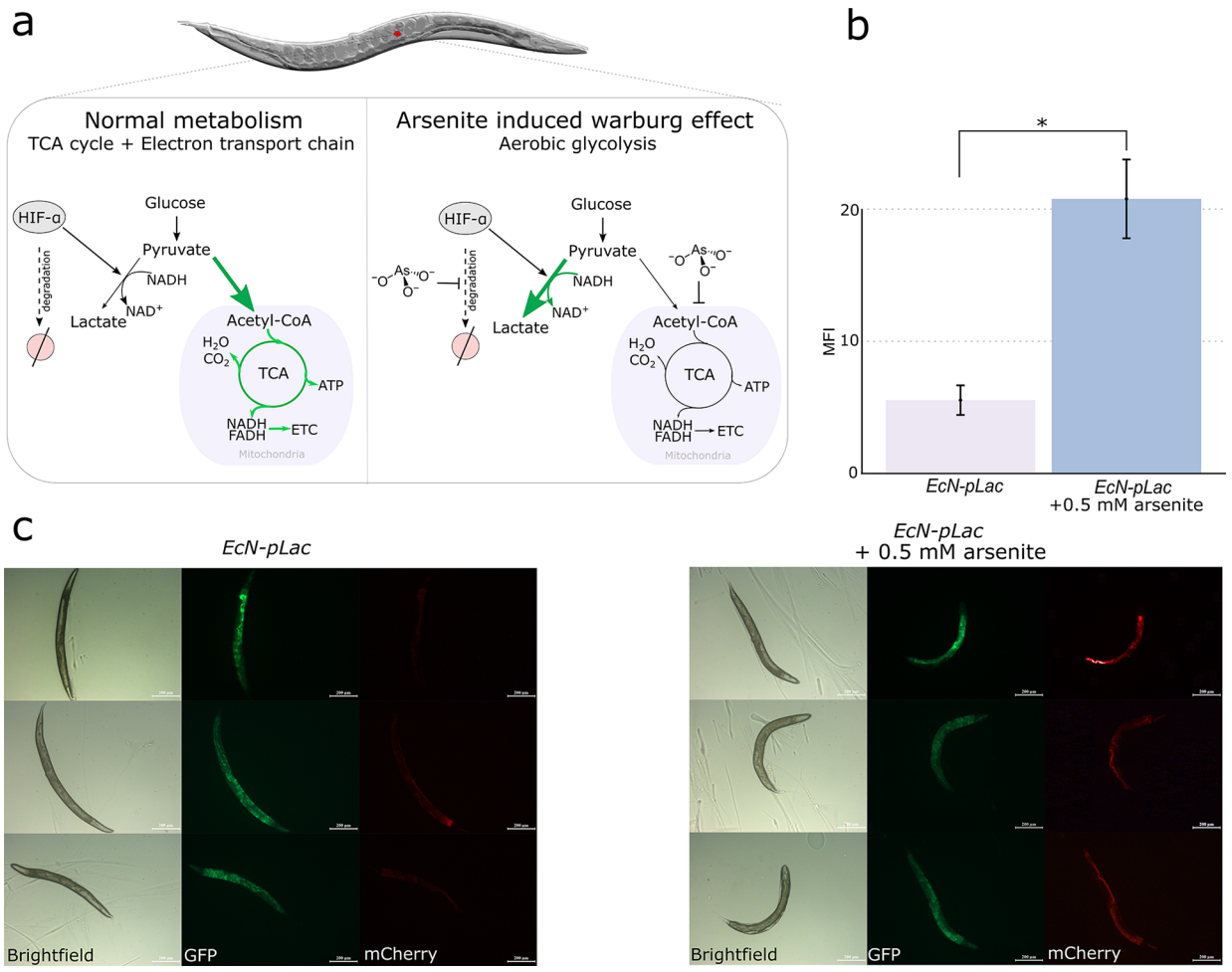

Figure 3. Detecting physiological changes in lactate concentrations in the intestinal environment of *C. elegans* upon exposure to arsenite. *C. elegans* N2 was colonized with lactate-sensing *EcN-pLac*. After 5 days of growth, adult worms were transferred to a fresh NGM plate or a NGM plate containing 0.5 mM arsenite. After 24 h, worms were analyzed using fluorescence microscopy. (a) Exposure to arsenite induces a Warburg-like effect by disrupting the membrane potential of the inner mitochondrial membrane and by preventing the breakdown of HIF-α, a positive regulator of the genes involved in glycolysis. The Warburg effect is characterized by an increased flux to glycolysis pathway and a buildup of lactate. (b) Mean pixel intensity was analyzed using ImageJ from red channel fluorescence. Significance determined using the paired *t*-test: $*p \leq 0.05$. (c) Brightfield, green and red channel fluorescence of worms ($n = 3$) colonized with *EcN-pLac* with and without exposure to arsenite (scale bar = 200 μM).

bacterial biosensors in *C. elegans* by demonstrating how a lactate biosensor can be used to report on changes in intestinal concentrations of lactate in response to arsenite exposure. Future work could build upon this concept and develop biosensors specifically for use in *C. elegans*, which could be a valuable research tool in this important model organism.

In summary, we characterized eight plasmid vectors for sensing relevant compounds and conditions found in the human GI tract and validated their performance in vivo using *C. elegans*. We believe that the vectors presented in this study will help expand the incorporation of more sensing elements in future work exploiting the probiotic EcN as a chassis for bacterial therapy and diagnostic tools.

MATERIALS AND METHODS

Strain Construction. The plasmids generated in this study were created with USER-cloning or Gibson assembly, using *E. coli* top 10 as the cloning host. The necessary transcription factors, promoters, and backbone plasmids were amplified with Q5 High-Fidelity DNA Polymerase (New England Biolabs) with uracil-containing primers where necessary. For USER cloning, purified polymerase chain reaction (PCR) fragments were treated with 0.5 μL of USER enzyme (NEB, Cat. No. M5505S) in 1× Cut Smart buffer (NEB, Cat. No. B7204S) and subsequently incubated for 30 min at 37 °C in a thermocycler and 1 h at room temperature. Then, 2 μL of this USER mixture was then used to transform One ShotTM TOP10 Chemically Competent *E. coli* (Thermofisher) according to the instruction of the supplier (One ShotTM TOP10 Thermofisher Catalog Numbers C4040-10). Gibson assembly was performed according to the instruction of the supplier (Gibson Assembly Protocol (E5510)). Transformed cells were plated on selective culture media, and colonies were verified with colony PCR and subsequent sequencing. A positive colony was inoculated into 2 mL of LB with 50 μg/mL kanamycin and grown for 16 h, after which the plasmid was extracted using a NucleoSpin Plasmid EasyPure extraction kit (Macherey Nagel, ref. 740727.250). Purified plasmid was used to transform electrocompetent cells of *E. coli* Nissle 1917 (Tn7:sfGFP$^+$, StrepR) by electroporation. sfGFP is integrated in the genome in an attTn7 attachment site at position 2672041 to 2672355, expressed from the BBa_J23101 promoter. The strain of EcN has previously been cured for

https://doi.org/10.1021/acssynbio.2c00491
ACS Synth. Biol. 2022, 11, 4184−4192

any native pMUT1 plasmid.[14] A detailed map of the plasmids together with the relevant sequences is available in Figure S7.

Chemical Inducers. The following chemicals were used as inducers in this study: lithium acetoacetate ≥90% purity from Sigma-Aldrich (A8509) dissolved in Milli-Q water, caffeine from Sigma-Aldrich (C0750) dissolved in Milli-Q water, sodium L-lactate ∼98% purity (L7022) dissolved in Milli-Q water, taurocholic acid sodium salt hydrate ≥95% purity from Sigma-Aldrich (T4009) dissolved in Milli-Q water, lithocholic acid ≥95% purity from Sigma-Aldrich (L6250) dissolved in dimethyl sulfoxide, and deoxycholic acid ≥98% purity from Sigma-Aldrich (D2510) dissolved in dimethyl sulfoxide. Δ^4-Dafachronic acid ≥95% purity from Cayman Chemicals (Item No. 14100) is dissolved in dimethyl sulfoxide.

Response Function in Aerobic Conditions. Glycerol stocks of EcN biosensor strains were inoculated in LB with relevant antibiotics and grown at 37 °C and 900 rpm overnight. Overnight cultures were diluted 1:100 in Greiner CELLSTAR 96-well microtiter plates (Sigma-Aldrich product number M0812) containing LB, 100 μg/mL streptomycin, and 50 μg/mL kanamycin spiked with various concentrations of inducer with a final working volume of 200 μL. The plate was sealed using a BreathEasy film (Sigma-Aldrich, St. Louis, MO, USA) and incubated in a Synergy H1 plate reader (BioTek, Winooski, VT, USA) at 37 °C, 1000 rpm. OD_{600}: mCherry (excitation 583 nm and emission 613 nm) and sfGFP (excitation 485 nm and emission 510 nm) for 40 h. All samples were grown in triplicate (n = 3), and kinetics were measured in 5 min intervals. The RFU of mCherry was normalized against the OD_{600} to consider any differences in growth arising from exposure to the inducer molecules. The normalized mCherry signal was used to compute the average response after 40 h of growth.

Response Function in Anaerobic Conditions. Glycerol stocks of EcN biosensor strains were streaked onto LB-agar plates containing 100 μg/mL streptomycin and 50 μg/mL kanamycin and acclimatized to anaerobic conditions for 16 h. A single colony was inoculated into liquid media and grown overnight. From this overnight culture, cells were diluted 1:100 in 2 mL Eppendorf tubes containing LB, 100 μg/mL streptomycin, and 50 μg/mL kanamycin spiked with various concentrations of inducer with a final working volume of 600 μL. Cells were allowed to grow for 40 h in a static incubator at 37 °C, after which 100 μg/mL of chloramphenicol was added to inhibit further growth and protein translation. Cells were transferred to a microtiter plate and read in a Synergy H1 plate reader as described for aerobic experiments. Anaerobic conditions were obtained using a Don Whitley A35 anaerobic workstation (gas mixture, 95% N_2 and 5% H_2) and moved to an airtight jar with an oxygen-absorbing pouch (GasPak EZ, 260683). All media used in anaerobic experiments were placed in anaerobic conditions for a minimum of 24 h prior to use, to allow the media to fully prereduce.

Response Function of the pH Sensor. Overnight cultures of *EcN-pCadBA* were reinoculated into 100 mM HEPES-LB buffered to pH 7 and grown to an OD_{600} of 0.3, after which the pH of the media was confirmed with pH strips. The cells were then collected and resuspended in fresh pH 7 buffered LB media and 100 mM acetic acid buffered LB adjusted to pH 5 and grown for 4 h after which the pH was confirmed to remain unchanged with pH strips. Followingly, cells were loaded to a microtiter plate and 100 μg/mL of chloramphenicol was added to inhibit further growth. The signal was monitored as previously described, and the pH was confirmed to remain unchanged with pH strips after 10 h.

Response Function of Oxygen Sensors. Overnight cultures of *EcN-pF8* and *EcN-pFF-41.5* were reinoculated into anaerobic and aerobic conditions, and samples were taken at 0, 1.5, 3, and 24 h. Immediately after sampling, chloramphenicol was added to inhibit any further growth or protein translation. The kinetics were followed until the mCherry signal had reached saturation and the expression was calculated from the normalized mCherry signal once the signal had saturated. Aerobic cultures were treated identically to allow direct comparison.

Computational Methods. The dose−response was modeled using a four-parameter log-logistic function in the DRC package in *R* with the model function displayed in eq 1.

$$f(x, (b, c, d, e) = c + \frac{d - c}{(1 + \exp(b(\log(x) - \log(e))))} \quad (1)$$

where b = steepness of the dose−response curve (cooperativity coefficient), $c = y_{max}$, $d = y_{min}$, $e = EC_{50}$, x = concentration of inducer, and $f(x, (b, c, d, e)$ = mean of normalized RFU calculated as from biological triplicates after 40 h of growth.

***C. elegans* Strains and Handling.** All experiments using *Caenorhabditis elegans* were carried out using the wild-type N2 Bristol strain, kindly provided by the CGC, which is funded by NIH Office of Research Infrastructure Programs (P40 OD010440). Worms were maintained at room temperature on NGM plates seeded with the auxotroph lab strain *E. coli* OP50 following standard procedures[42] unless stated otherwise.

EcN Biosensor Colonization and Induction in *C. elegans*. First, 5−10 adult worms were transferred from OP50-seeded NGM plates to NGM plates seeded with EcN biosensors and allowed to proliferate. After 5 days, adult worms were washed and transferred either to fresh unseeded NGM plates (negative controls) or unseeded plates containing the relevant inducer (20 mM acetoacetate, 100 mM lactate, 186 mM taurocholic acid, 77 μM caffeine, 5.2 mM deoxycholic acid, and 3.2 mM lithocholic acid). After 24 h of induction, worms were washed and transferred to Greiner Bio-One 6-well cell culture plates (Item No.: 657160) containing 200 μL of NGM agar with 0.2% levamisole as the anesthetic. Worms were imaged using a IncuCyte S3 Live-Cell Analysis System with a 4× objective and 300 ms exposure for red and green fluorescence images. Pixel intensity was measured using ImageJ.

Fluorescence Microscopy of *C. elegans*. Animals were mounted on 2% agar pads containing 0.2% levamisole as the anesthetic and imaged using a Leica DM4000 with a 20× objective and a Leica DFC300 FX Digital Color Camera.

■ ASSOCIATED CONTENT

Supporting Information

The Supporting Information is available free of charge at https://pubs.acs.org/doi/10.1021/acssynbio.2c00491.

Schematic representation of the pMUT1 biosensor plasmid, characterization of *EcN-pCaf* in exposure to theophylline, performance of *EcN-pCadBA* at pH 7 spiked with acetic acid, activation of *EcN-VtrA* by dafachronic acid, fluorescence microscopy images of *C. elegans* colonized with *EcN-pCadBA*, characterization of

https://doi.org/10.1021/acssynbio.2c00491
ACS Synth. Biol. 2022, 11, 4184−4192

EcN-pLac in exposure to arsenite in vitro, and detailed plasmid maps and sequences used in this study (PDF)

AUTHOR INFORMATION

Corresponding Authors

Ruben Vazquez-Uribe − *Novo Nordisk Foundation Center for Biosustainability, Technical University of Denmark, 2800 Kongens Lyngby, Denmark*; Email: ruvas@biosustain.dtu.dk

Morten Otto Alexander Sommer − *Novo Nordisk Foundation Center for Biosustainability, Technical University of Denmark, 2800 Kongens Lyngby, Denmark*; orcid.org/0000-0003-4005-5674; Email: msom@bio.dtu.dk

Author

Troels Holger Vaaben − *Novo Nordisk Foundation Center for Biosustainability, Technical University of Denmark, 2800 Kongens Lyngby, Denmark*

Complete contact information is available at: https://pubs.acs.org/10.1021/acssynbio.2c00491

Author Contributions

T.H.V., R.V.U., and M.O.A.S. conceived the study, and all authors contributed to the study's design. T.H.V. carried out all experiments. T.H.V. analyzed the data and wrote the manuscript. R.V.U. and M.O.A.S. supervised the study. All authors contributed to the discussion of the results. All authors read and approved the final manuscript.

Notes

The authors declare no competing financial interest.

ACKNOWLEDGMENTS

This work received funding from The Novo Nordisk Foundation under NNF Grant No. NNF20CC0035580 and NNF Challenge program CAMiT under Grant No. NNF17CO0028232. The authors would like to thank Mogens Kilstrup, Karl Alex Hedin, and Carola Elisa Heesemann Rosenkilde for guidance on the experimental design and discussion of the manuscript and Christian Højte Schouw for providing a script for the data processing.

REFERENCES

(1) Malla, M. A.; Dubey, A.; Kumar, A.; Yadav, S.; Hashem, A.; Allah, E. F. A. Exploring the human microbiome: The potential future role of next-generation sequencing in disease diagnosis and treatment. *Front. Immunol.* **2019**, *10*, 2868.

(2) Cubillos-Ruiz, A.; Guo, T.; Sokolovska, A.; et al. Engineering living therapeutics with synthetic biology. *Nat. Rev. Drug Discovery* **2021**, *20*, 941−960.

(3) Davani-Davari, D.; Negahdaripour, M.; Karimzadeh, I.; et al. Prebiotics: Definition, Types, Sources, Mechanisms, and Clinical Applications. *Foods* **2019**, *8*, 92.

(4) van Nood, E.; Vrieze, A.; Nieuwdorp, M.; et al. Duodenal Infusion of Donor Feces for Recurrent Clostridium difficile. *N. Engl. J. Med.* **2013**, *368*, 407−415.

(5) Charbonneau, M. R.; Isabella, V. M.; Li, N.; Kurtz, C. B. Developing a new class of engineered live bacterial therapeutics to treat human diseases. *Nat. Commun.* **2020**, *11*, 1−11.

(6) Whelan, R. A.; Rausch, S.; Ebner, F.; et al. A transgenic probiotic secreting a parasite immunomodulator for site-directed treatment of gut inflammation. *Mol. Ther.* **2014**, *22*, 1730−1740.

(7) Isabella, V. M.; Ha, B. N.; Castillo, M. J.; et al. Development of a synthetic live bacterial therapeutic for the human metabolic disease phenylketonuria. *Nat. Biotechnol.* **2018**, *36*, 857−864.

(8) Yu, X.; Lin, C.; Yu, J.; Qi, Q.; Wang, Q. Bioengineered *Escherichia coli* Nissle 1917 for tumour-targeting therapy. *Microb. Biotechnol.* **2020**, *13*, 629.

(9) Amrofell, M. B.; Rottinghaus, A. G.; Moon, T. S. Engineering microbial diagnostics and therapeutics with smart control. *Curr. Opin. Biotechnol.* **2020**, *66*, 11.

(10) Rottinghaus, A. G.; Amrofell, M. B.; Moon, T. S. Biosensing in Smart Engineered Probiotics. *Biotechnol. J.* **2020**, *15*, No. 1900319.

(11) Chang, H. J.; Zúñiga, A.; Conejero, I.; et al. Programmable receptors enable bacterial biosensors to detect pathological biomarkers in clinical samples. *Nat. Commun.* **2021**, *12*, 1−12.

(12) Courbet, A.; Endy, D.; Renard, E.; Molina, F.; Bonnet, J. Detection of pathological biomarkers in human clinical samples via amplifying genetic switches and logic gates. *Sci. Transl. Med.* **2015**, *7*, 289ra83.

(13) Inda, M.; Jimenez, M.; Liu, Q.; et al. Ingestible capsule for detecting labile inflammatory biomarkers in situ. *bioRxiv* **2022**, No. 480562.

(14) Armetta, J.; Schantz-Klausen, M.; Shepelin, D.; et al. *Escherichia coli* Promoters with Consistent Expression throughout the Murine Gut. *ACS Synth. Biol.* **2021**, *10*, 3359−3368.

(15) d'Oelsnitz, S.; Ellington, A. D. GroovDB: A database of ligand-inducible transcription factors. *bioRxiv* **2022**, No. 500503.

(16) Hossain, G. S.; Saini, M.; Miyake, R.; Ling, H.; Chang, M. W. Genetic Biosensor Design for Natural Product Biosynthesis in Microorganisms. *Trends Biotechnol.* **2020**, *38*, 797−810.

(17) Rugbjerg, P.; Sommer, M. O. A. Overcoming genetic heterogeneity in industrial fermentations. *Nat. Biotechnol.* **2019**, *37*, 869−876.

(18) Kan, A.; Gelfat, I.; Emani, S.; Praveschotinunt, P.; Joshi, N. S. Plasmid Vectors for in Vivo Selection-Free Use with the Probiotic *E. coli* Nissle 1917. *ACS Synth. Biol.* **2021**, *10*, 94−106.

(19) Rutter, J. W.; Dekker, L.; Fedorec, A. J. H.; et al. Engineered acetoacetate-inducible whole-cell biosensors based on the AtoSC two-component system. *Biotechnol. Bioeng.* **2021**, *118*, 4278−4289.

(20) Chien, T.; Harimoto, T.; Kepecs, B.; et al. Enhancing the tropism of bacteria via genetically programmed biosensors. *Nat. Biomed. Eng.* **2022**, *6*, 94−104.

(21) Chang, H. J.; Mayonove, P.; Zavala, A.; et al. A Modular Receptor Platform to Expand the Sensing Repertoire of Bacteria. *ACS Synth. Biol.* **2018**, *7*, 166−175.

(22) Barnard, A. M. L.; Green, J.; Busby, S. J. W. Transcription Regulation by Tandem-Bound FNR at *Escherichia coli* Promoters. *J. Bacteriol.* **2003**, *185*, 5993.

(23) Moser, F.; Borujeni, A. E.; Ghodasara, A. N.; Cameron, E.; Park, Y.; Voigt, C. A. Dynamic control of endogenous metabolism with combinatorial logic circuits. *Mol. Syst. Biol.* **2018**, *14*, e8605.

(24) Haneburger, I.; Eichinger, A.; Skerra, A.; Jung, K. New Insights into the Signaling Mechanism of the pH-responsive, Membrane-integrated Transcriptional Activator CadC of *Escherichia coli*. *J. Biol. Chem.* **2011**, *286*, 10681.

(25) Zúñiga, A.; Camacho, M.; Chang, H. J.; et al. Engineered L-Lactate Responding Promoter System Operating in Glucose-Rich and Anoxic Environments. *ACS Synth. Biol.* **2021**, *10*, 3527−3536.

(26) Stephens, J. M.; Sulway, M. J.; Watkins, P. J. Relationship of Blood Acetoacetate and 3-Hydroxybutyrate in Diabetes. *Diabetes* **1971**, *20*, 485−489.

(27) Belenguer, A.; Duncan, S. H.; Holtrop, G.; Anderson, S. E.; Lobley, G. E.; Flint, H. J. Impact of pH on lactate formation and utilization by human fecal microbial communities. *Appl. Environ. Microbiol.* **2007**, *73*, 6526−6533.

(28) Humbert, L.; Rainteau, D.; Tuvignon, N.; et al. Postprandial bile acid levels in intestine and plasma reveal altered biliary circulation in chronic pancreatitis patients. *J. Lipid Res.* **2018**, *59*, 2202−2213.

(29) Ohmichi, T.; Kasai, T.; Shinomoto, M.; et al. Quantification of Blood Caffeine Levels in Patients With Parkinson's Disease and Multiple System Atrophy by Caffeine ELISA. *Front. Neurol.* **2020**, *11*, 1774.

(30) Keller, S.; Jahreis, G. Determination of underivatised sterols and bile acid trimethyl silyl ether methyl esters by gas chromatography-mass spectrometry-single ion monitoring in faeces. *J. Chromatogr. B: Anal. Technol. Biomed. Life Sci.* **2004**, *813*, 199−207.
(31) Rutter, J. W.; Ozdemir, T.; Galimov, E. R.; et al. Detecting Changes in the Caenorhabditis elegans Intestinal Environment Using an Engineered Bacterial Biosensor. *ACS Synth. Biol.* **2019**, *8*, 2620−2628.
(32) Poupet, C.; Chassard, C.; Nivoliez, A.; Bornes, S. Caenorhabditis elegans, a Host to Investigate the Probiotic Properties of Beneficial Microorganisms. *Front. Nutr.* **2020**, *7*, 135.
(33) Luz, A. L.; Godebo, T. R.; Bhatt, D. P.; et al. From the Cover: Arsenite Uncouples Mitochondrial Respiration and Induces a Warburg-like Effect in Caenorhabditis elegans. *Toxicol. Sci.* **2016**, *152*, 349−362.
(34) Salzer, L.; Witting, M. Quo Vadis Caenorhabditis elegans Metabolomics—A Review of Current Methods and Applications to Explore Metabolism in the Nematode. *Metabolites* **2021**, *11*, 284.
(35) Ravcheev, D. A.; Gerasimova, A. V.; Mironov, A. A.; Gelfand, M. S. Comparative genomic analysis of regulation of anaerobic respiration in ten genomes from three families of gamma-proteobacteria (Enterobacteriaceae, Pasteurellaceae, Vibrionaceae). *BMC Genomics* **2007**, *8*, 54.
(36) Mandin, P.; Gottesman, S. Integrating anaerobic/aerobic sensing and the general stress response through the ArcZ small RNA. *EMBO J.* **2010**, *29*, 3094−3107.
(37) Dimov, I.; Maduro, M. F. The C. elegans intestine: organogenesis, digestion, and physiology. *Cell Tissue Res.* **2019**, *377*, 383−396.
(38) Chan, J. P.; Wright, J. R.; Wong, H. T.; et al. Using Bacterial Transcriptomics to Investigate Targets of Host-Bacterial Interactions in Caenorhabditis elegans. *Sci. Rep.* **2019**, *9*, 5545.
(39) Ayoade, K. O.; Carranza, F. R.; Cho, W. H.; et al. Dafachronic acid and temperature regulate canonical dauer pathways during Nippostrongylus brasiliensis infectious larvae activation. *Parasites Vectors* **2020**, *13*, 162.
(40) Ma, G.; Wang, T.; Korhonen, P. K.; et al. Dafachronic acid promotes larval development in Haemonchus contortus by modulating dauer signalling and lipid metabolism. *PLoS Pathog.* **2019**, *15*, No. e1007960.
(41) Aguilaniu, H.; Fabrizio, P.; Witting, M. The Role of Dafachronic Acid Signaling in Development and Longevity in Caenorhabditis elegans: Digging Deeper Using Cutting-Edge Analytical Chemistry. *Front. Endocrinol.* **2016**, *7*, 12.
(42) Stiernagle, T. Maintenance of *C. elegans*. *WormBook* **2006**, 1−11.

https://doi.org/10.1021/acssynbio.2c00491
ACS Synth. Biol. 2022, 11, 4184−4192